ACS APPLIED MATERIALS & INTERFACES
Research Article
www.acsami.org

Enhanced Hole Injection in Phosphorescent Organic Light-Emitting Diodes by Thermally Evaporating a Thin Indium Trichloride Layer

Chun-Hong Gao, Shi-Duan Cai, Wei Gu, Dong-Ying Zhou, Zhao-Kui Wang,* and Liang-Sheng Liao*

Jiangsu Key Laboratory for Carbon-Based Functional Materials & Devices, Institute of Functional Nano & Soft Materials (FUNSOM), Soochow University, Suzhou, Jiangsu 215123, China

Ⓢ *Supporting Information*

ABSTRACT: An ultrathin layer of indium trichloride ($InCl_3$) is thermally evaporated on the indium tin oxide (ITO) anode to enhance the hole injection in simplified phosphorescent organic light-emitting diodes (PHOLEDs). Comparing with the device with ultraviolet (UV)-ozone treatment, the device modified by $InCl_3$ exhibits a maximum current efficiency of 82.2 cd/A measured at about 2000 cd/cm^2 and 36% improvement in power efficiency measured at 20 mA/cm^2. More importantly, more than three times improvement in half lifetime estimated at an initial luminance of 1000 cd/cm^2 is achieved. The investigations using ultraviolet photoelectron spectroscopy, X-ray photoelectron spectroscopy, and the bias- and temperature-dependent current density−voltage characteristics in the related hole-dominated devices have revealed that the improved device performance is mainly attributed to the enhanced hole injection resulting from the lowered hole injection barrier height in the $InCl_3$-modified devices.

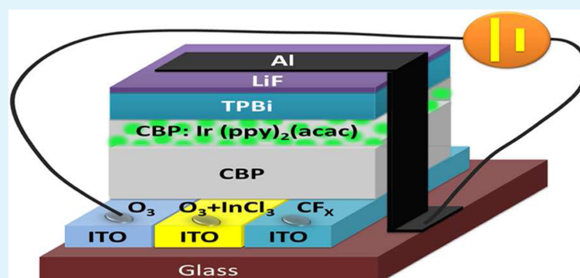

KEYWORDS: *phosphorescent OLEDs, hole injection, indium trichloride, surface modification, thermal evaporation, work function*

1. INTRODUCTION

Since the first organic light-emitting diode (OLED) was reported in the 1980s,[1] significant progress has been made in improving the device efficiency and lifetime through device engineering with balanced electron and hole injection from electrodes.[2,3] Large energy barrier between electrodes and organic materials would cause high operation voltage, low-efficiency electroluminescence (EL), and fast degradation in OLEDs.[4−7] The most commonly used OLED anode material, indium tin oxide (ITO), has high transparency and conductivity, while its relatively low work function (∼4.7 eV) is ∼1 eV lower than the energy-levels of active organic materials. Some complicated methods for ITO modification are proposed to reduce the barrier height and facilitate hole injection, such as oxygen plasma treatment,[8] ultraviolet (UV)-ozone treatment,[9] thermal annealing,[10] and self-assembling.[11] In addition, a potential strategy to improve the hole injection is to insert an additional hole injection layer (HIL) between ITO and the hole transport layer (HTL). For example, copper phthalocyanine (CuPc),[12] hexaazatriphenylene-hexacarbonitrile (HAT-CN),[13] transition metal oxide (MoO_3, V_2O_5, WO_3, NiO),[14−17] poly(3, 4-ethylenedioxythiophene) (PEDOT),[18] CF_x,[19,20] and p-type doping layer[21] have been used successfully in OLEDs for improving hole injections. For example, Hung et al. demonstrated that CF_x formed by a low frequency plasma-assisted polymerization of CHF_3 on ITO surface can enhance both the device efficiency and the lifetime of OLEDs.[13,18] However, the treatments of oxygen plasma and UV-ozone will increase the surface oxygen concentration, and cause the oxidation of the adjacent material, which is not favorable to the stability of the device.[22] For CF_x treatment, it is difficult to control the "x" value causing unsatisfied reproducibility. Moreover, fabrication complexity will be introduced when using doping technique. Additionally, the thermal evaporation temperature of transition metal oxide is usually higher than 800 °C,[3] which is not suitable for low-cost production of OLEDs from a manufacturing perspective.

Recently, Helander et al.[23] and Cao et al.[24] reported that the work function of ITO can be dramatically raised via treatments of UV-ozone combined with *o*-dichlorobenzene and/or Cl_2 plasma owing to directly forming In−Cl bonds at the surface. However, besides additional equipment, it is hard to control the treatment environment such as temperature, humidity and concentration in different places. A vacuum evaporated technique may overcome these issues when introducing the thin $InCl_3$ layer. In this work, we introduce a vacuum evaporated $InCl_3$ layer into the phosphorescent organic light-emitting diodes (PHOLEDs) for improving the hole injection. A maximum 36% improvement in power efficiency at 20 mA/cm^2 and three times improvement in half lifetime were achieved comparing with the device with UV-ozone treatment. The measurement of photoelectron spectroscopy revealed that the work function of ITO was increased from 4.90 to 5.38 eV. And the reduced barrier height of hole injection was further verified

Received: June 22, 2012
Accepted: September 24, 2012
Published: September 24, 2012

© 2012 American Chemical Society

by the bias- and temperature-dependent current density–voltage (J–V) characteristics in the hole-dominated devices.

2. EXPERIMENTAL SECTION

The materials used in this work are 4′-bis(carbazol-9-yl)biphenyl (CBP), 2,2′,2″-(1,3,5-benzinetriyl)-Tris(1-phenyl-1-H-benzimidazole) (TPBi), bis(2-phenylpyridine)(acetylacetonate)iridium(III) (Ir(ppy)$_2$(acac)), InCl$_3$, LiF, and Al. All the materials have the purity higher than 99% and are used without further purification. The molecular structures of the organic materials can be found elsewhere.[23] OLEDs are fabricated on commercially available glass substrates precoated with an ITO layer having a thickness of ~110 nm and a sheet resistance of 15 Ω/square under a base pressure of 2×10^{-6} Torr. The device structure (shown in Figure 1) is: ITO (with different treatments)/CBP (35 nm)/CBP: Ir(ppy)$_2$(acac) 8 wt % (15 nm)/TPBi (65 nm)/LiF (1 nm)/Al (150 nm), where CBP is used as both a hole transport layer and a host layer, TPBi is used as an electron transport layer, LiF/Al is used as a bilayer cathode. All the ITO anodes are cleaned with standard process: brushing with detergent and then ultrasonic cleaning in acetone, ethanol and deionized water in sequence. Three devices are fabricated on the as-cleaned ITO anode after different treatments: Device A with 15 min UV-ozone treatment, Device B with 15 min UV-ozone treatment and 1 nm thermally deposited InCl$_3$, Device C with 1 nm CF$_x$ deposited by plasma-assisted deposition of CHF$_3$ (The thickness optimization of InCl$_3$ can be seen in Figure S1 in the Supporting Information, and the surface morphologies of the devices with or without 1 nm InCl$_3$ can be seen in Figure S3 in the Supporting Information). The electroluminescence (EL) characteristics are measured using a constant current source (Keithley 2400 SourceMeter) with a photometer (Photo Research SpectraScan PR 655). The active area of each device is 0.1 cm^2. The half lifetime (T_{50} defined as the duration from the start of testing to the time at which luminance is reduced to 50% of its initial value in given testing conditions) and the drive voltage are measured at a constant current density of 20 mA/cm^2.

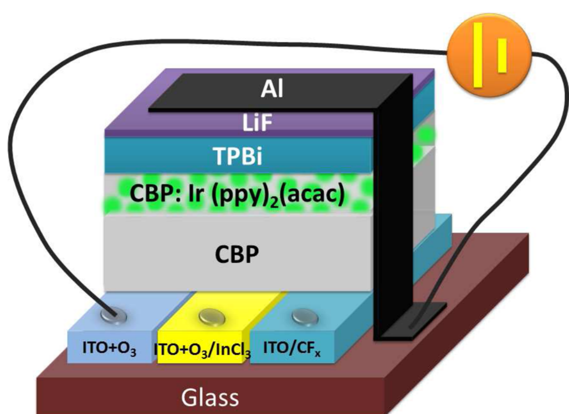

Figure 1. Schematic device structure of green phosphorescent organic light-emitting diodes in this work.

The hole injection characteristics in the three devices with different treatment were investigated using ultraviolet photoelectron spectroscopy (UPS) and X-ray photoelectron spectroscopy (XPS) in a Kratos AXIS Ultra^{DLD} ultrahigh vacuum (UHV) surface analysis system, consisting of a multiport carousel chamber and an analysis chamber with a base pressure of 5×10^{-10} and 3×10^{-10} Torr, respectively. The UPS measurements were carried out with an unfiltered HeI (21.2 eV) gas discharge lamp to characterize the work function. For collection of secondary electrons, the samples are negatively biased at 4 V. The XPS measurements on elemental composition and chemical state information were performed using a monochromatic aluminum K$_\alpha$ source (1486.6 eV). All measurements were carried out at room temperature. The photoelectrons are collected by a hemispherical analyzer with a total instrumental energy resolution of 0.1 eV for the UPS measurements and 0.5 eV for the XPS measurements. In all UPS and XPS spectra, the Fermi level (E_F) is referred as the zero binding energy (BE).

Two hole-dominated devices (Device E and Device F) with a structure of "anode/CBP (60 nm) /Al (100 nm)" were fabricated for evaluating the temperature dependence of J–V characteristics in the temperature range of 210–290 K. The anode of Device E was treated with only UV-ozone (15 min), but that of Device F was treated with UV-ozone (15 min) followed by adding 1 nm InCl$_3$. The properties were characterized in a cryogenic probe station (Lake Shore, CRX-4 K) connected to a Keithley 4200-SCS semiconductor parameter analyzer.

3. RESULTS AND DISCUSSION

3.1. Device EL Characteristics. The EL performance of Devices A, B and C is shown in Figure 2. Figure 2a shows the J–V and luminance–voltage (L–V) characteristics of the three devices. Device B with 1 nm InCl$_3$ exhibits the largest current density and the highest luminance at each specific drive voltage. The three devices have the identical EL spectra (shown in the inset of Figure 2a) originated from the dopant material Ir(ppy)$_2$(acac), which means that the radiation recombination zone is well confined within the light-emitting layer. Figure 2b

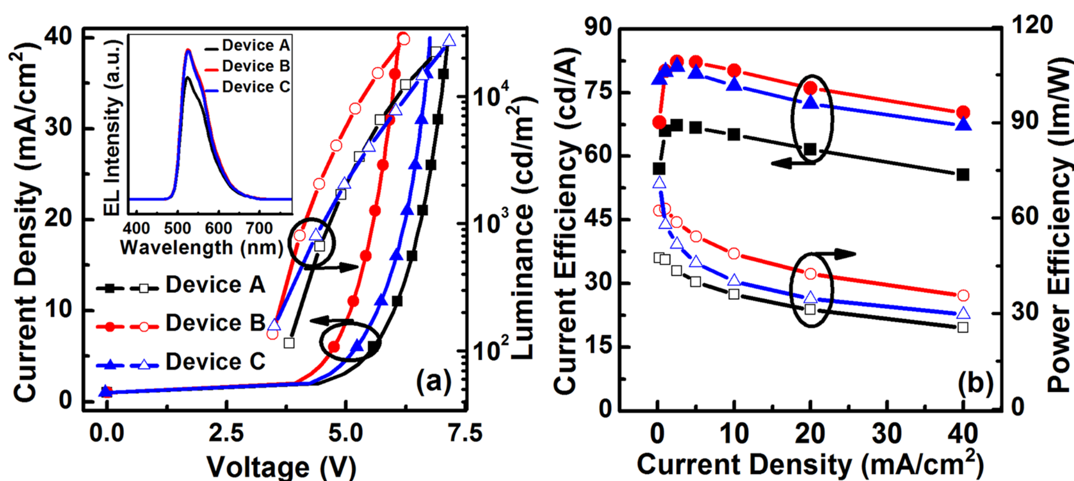

Figure 2. EL performance of OLED Devices A, B, and C. (a) Current density–voltage–luminance curves. (b) Current efficiency–current density–power efficiency curves. The electroluminance intensity versus wavelength is shown in the inset of a.

shows the current efficiency and power efficiency characteristics of the three devices. Device B with 1 nm $InCl_3$ exhibits the best current efficiency and power efficiency with reduced efficiency roll-off. At 20 mA/cm^2, the current efficiency and power efficiency for Devices A, B and C are 61.6, 76, and 72.3 cd/A, and 31.0, 42.4, and 34.6 lm/W, respectively. Device B modified by 1 nm $InCl_3$ exhibits 36% improvement in power efficiency at 20 mA/cm^2. Moreover, Device B shows a maximum current efficiency of 82.2 cd/A at 2057 cd/cm^2. Specifically, in whole luminance range (0.2−40 mA/cm^2), over 30% improvement in power efficiency is achieved compared to Device A. In particular, Device B also shows a better EL performance than the reference Device C, which is treated by CF_x plasma.

3.2. Enhanced Hole Injection. *3.2.1. In−Cl Dipole Formation Detected by XPS.* To understand the underlying mechanism of improved EL performance, we carried out XPS analysis of the ITO anodes in Devices A and B. Figure 3 shows

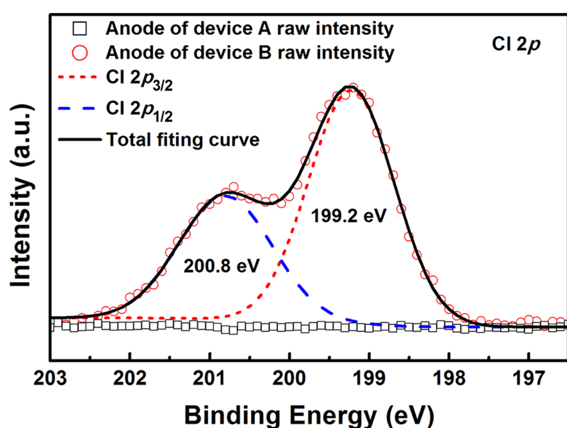

Figure 3. Cl 2p core levels of tested intensity and the fitted spectra for ITO anodes of Devices A (without $InCl_3$) and B (with 1 nm $InCl_3$).

the Cl 2p core levels of the ITO anode in Devices A and B, corresponding to without and with 1 nm $InCl_3$, respectively. In Device A, the ITO anode is free of Cl, whereas a strong Cl 2p signal consisting of Cl $2p_{3/2}$ and Cl $2p_{1/2}$ appears for the ITO in Device B. To determine the nature of the Cl chemical bond, we examined the XPS spectra of the Cl 2p core level with high resolution. Only a single chemical species of Cl is present after a fitting by single doublet peak. The Cl 2p binding energy of this species is 199.2 and 200.8 eV, which rules out chlorate and perchlorate.[25] This means that the Cl 2p core level is identical to $InCl_3$.[23]

The normalized spectra of In 3d core level for ITO anodes in Devices A and B are shown in Figure 4. For the ITO in Device B, In 3d core level band is broaden which can be decomposed into two components corresponding to In−O bonds (445.1 eV) and In^{3+}−Cl^- bonds (446.0 eV).[26] The In^{3+}−Cl^- (446.0 eV) bonds are more stable than the mixture of In−Cl bonds (~445.8 eV, comprised of In^+−Cl^- and In^{3+}−Cl^-) originated from the treatments of Cl_2 plasma[24] and the vapor *o*-dichlorobenzene.[23] On the basis of common UPS analysis, the work function of ITO is strongly influenced by the electrostatic conditions at its surface. Therefore, by using polar molecules such as $InCl_3$ on ITO with the dipole oriented outward from the surface, a thin dipolar layer is formed and the work function can be manipulated. Therefore, we believe that the formation of In^{3+}−Cl^- bonds would attribute to the increase of the work function. In the following subsection, we will indicate that our

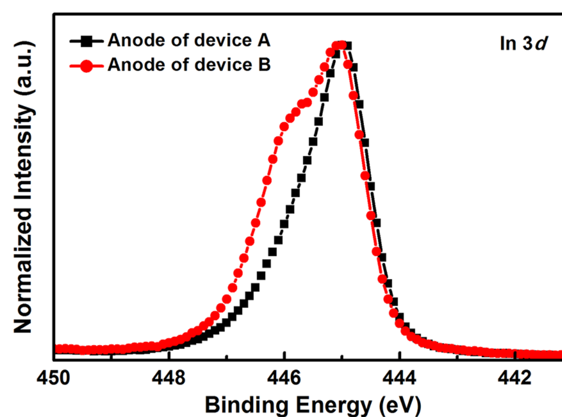

Figure 4. Normalized In 3d core level spectra for ITO anodes of Devices A (without $InCl_3$) and B (with 1 nm $InCl_3$).

results are consistent with the theory proposed by Helander et al.[23] and Cao et al.,[24] in which the polarized In−Cl bonds formed at the ITO surface introduce a layer of dipoles, resulting in the raising of the vacuum energy level and thus the ITO work function. The barrier height of hole injections from the ITO to the HOMO of CBP can be reduced by an $InCl_3$ modification. Thus, holes are easily injected into the light-emitting region in Device B and less accumulated at the interface of ITO/CBP, resulting in reduced turn-on voltage by ~1 V in Device B compared to that of Device A. Therefore, Device B exhibits the better EL performance than Device A.

3.2.2. Work Function of ITO with Different Treatments. As aforementioned, to further understand the injection mechanism and quantitatively confirm the cause of the enhancement of efficiency, the work function of ITO anode with different treatments is studied using UPS. As shown in Figure 5, the

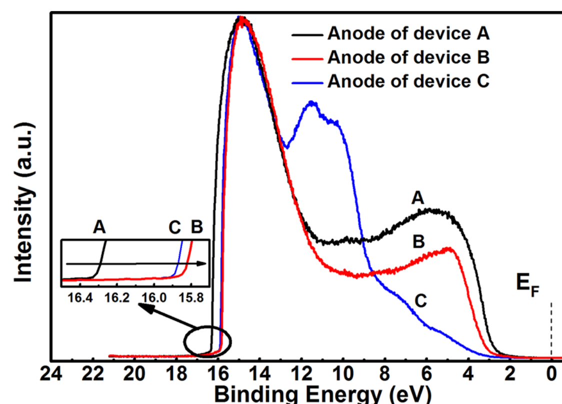

Figure 5. UPS spectra of different ITO anodes of Devices A, B, and C. The inset is the magnification of the secondary electron cutoff edge.

secondary cutoffs of the UPS spectra demonstrate that the work function of ITO has been improved from 4.90 to 5.38 and 5.32 eV for $InCl_3$ modification and CF_x treatment, respectively.

As is known, the high energy UV of UPS measurement may cause degradation for ITO samples, leading to a lower measuring value of the work function by about 0.5 eV.[27,28] Therefore, it will cause inaccuracy to the analysis of carrier injection barrier height at the ITO/organic interface (e.g., ITO/CBP). However, we mainly focused on the difference of the barrier height, instead of the absolute value of the barrier height at the ITO/CBP interface with differently treated ITO

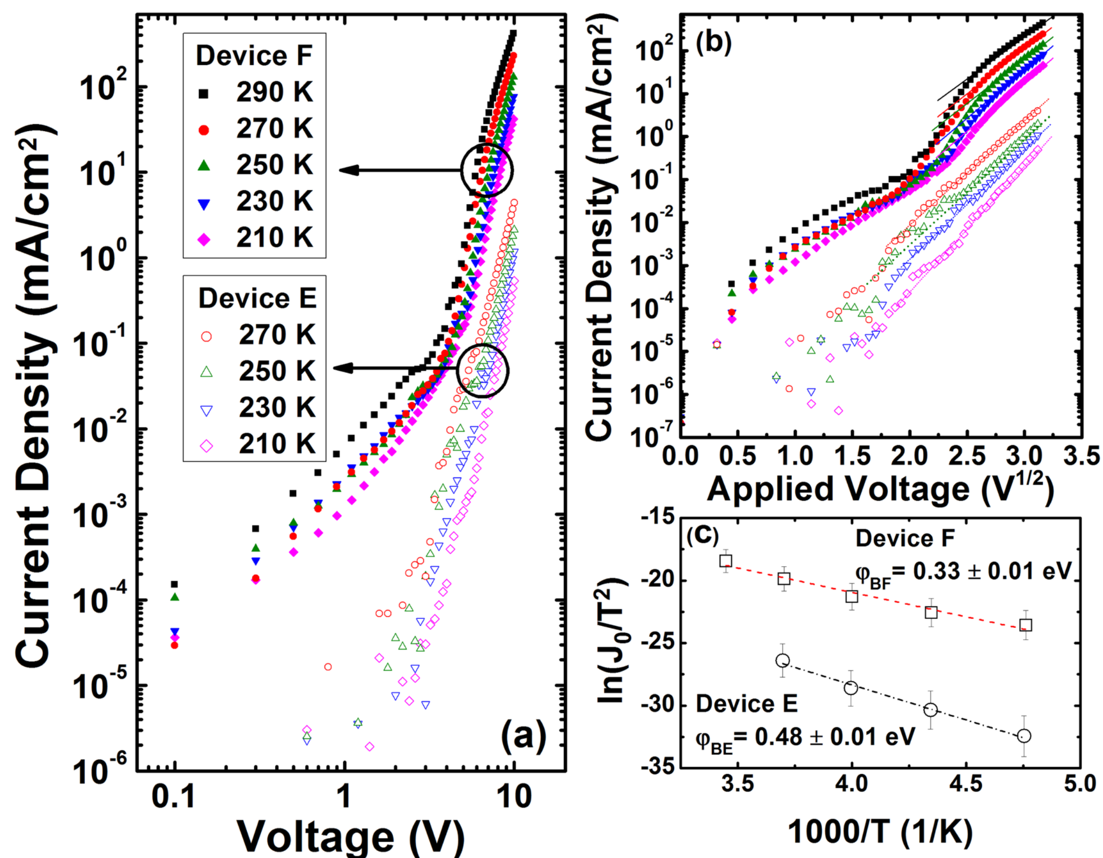

Figure 6. (a) Temperature-dependent J–V characteristics of Device E (without $InCl_3$) and Device F (with 1 nm $InCl_3$); (b) relationship between ln$J$ and $V^{1/2}$ of Devices E and F; (c) relationships between lnJ_0/T^2 and $1/T$ of Devices E and F. J_0 is obtained by extrapolating in $V = 0$.

substrate in this work. Therefore, although the barrier heights at the ITO/CBP interfaces measured by the UPS may be inaccurate, the difference in the barrier heights could be relatively accurate in considering that the UV exposure for all the samples are the same.

Nevertheless, the hole injection barrier of the ITO with 1 nm $InCl_3$ modification can be reduced compared with that of ITO with only UV-ozone treatment. In Device A, the highest occupied molecular orbital (HOMO) of host materials CBP is too deep to directly inject holes from ITO so that many holes are accumulated at the interface of the ITO and CBP, which leads to additional voltage drop at ITO/CBP interface. As a result, Device A exhibits the highest drive voltage and the lowest efficiency among the three devices. Therefore, additional modifications are required to match the energy-levels of organic materials to the low work function of ITO. In present work, the work function of ITO modified by 1 nm $InCl_3$ and CF_x plasma can be improved to 5.38 and 5.32 eV, respectively, resulting in a better energy alignment between ITO and organic materials, and hence the lower drive voltage and higher efficiency of Devices B and C.

3.2.3. Injection Barrier of Holes. To know the difference of the hole-injection barrier heights between the devices using differently treated ITO substrates, two hole-dominated devices (without (Device E) and with 1 nm $InCl_3$ (Device F) are fabricated. The temperature-dependent J–V characteristics in Device E and F are shown in Figure 6a. For device without $InCl_3$ (Device E), J increases smoothly with drive voltage under whole voltage range in a slop of about 6. In device with $InCl_3$ (Device F), three distinct regions are seen in a log–log representation in Device F. In the low bias region (<4.2 V), the slop is about 2 and the temperature dependence of current density is obvious. In the middle bias region (4.3–6.4 V), the current density increases rapidly with voltage in a slop of about 10 because of increased traps. In the high bias region (>6.3 V), a smooth increasing trend in current density appears with a slop of about 6 after a sharp increase. Particularly, the current density is increased with 2 orders of magnitude in Device F compared with that in Device E at the same voltage and identical temperature. In addition, obvious temperature dependence of J–V characteristics in two devices is observed in this region. Usually, the dominant parameter that controls the injection current is the height of the Schottky barrier. And an obvious temperature dependence of J–V characteristics is associated with a Schottky thermal emission current at a certain extent.[5,29,30] Experimentlly, the charge injection processes from a metal into an insulator or semiconductor are qualitatively analyzed, however, the quantitative details are less established due to the complexity of the interface caused by chemical, structural and morphological factors which affect strongly the charge injection process.[31] In particular, the charge injection at metal/organic interface is also dependent on the mobility of organic materials, which has shown clearly in the experiments of Shen et al.[32] In present cases, two hole-dominated devices without additional electron blocking layer (CBP/Al interface is good enough to guarantee a hole-dominated device) were fabricated to qualitatively evaluate the hole barrier conditions in order to decrease the potential effects of excessive interfaces and mobility dependence for additional organic material.[31]

The temperature-dependent $J-V$ curves in high bias region (>6.3 V) in Devices E and F is fitted by a Schottky thermal emission model[31,33]

$$J = AT^2 \exp\left[\frac{-q\left(\varphi_B - \sqrt{\frac{qV}{4\pi\varepsilon_i d}}\right)}{kT}\right] \quad (2)$$

where A^* is the effective Richardson constant, T the temperature, φ_B the barrier height at the interface, q the electronic charge, V the applied voltage, ε_i the dielectric permittivity of the mixed organic layer, d the thickness of organic layer, and k the Boltzmann constant. In Figure 6b, the $J-V$ characteristics are plotted with the relationship $\ln J$ vs $V^{1/2}$. By extrapolating straight lines to the ordinal point, the current densities J_0 at zero voltage under different temperature are determined. Using the determined J_0 values, the relationship between $\ln J_0/T^2$ vs $1/T$ is plotted, as shown in Figure 6c. The slope of the extrapolated line gives a barrier height of 0.48 and 0.33 eV for hole injection in Devices E and F, respectively. The barrier height of hole injection is reduced by 0.15 eV after thermally evaporating 1 nm $InCl_3$ onto the ITO. The barrier height derived from the temperature-dependent measurements is not equal to the difference between the work functions of the ITO electrode and the energy level of the adjacent organic materials. It implies that some changes occurred at the interfaces of different treated ITO/organic material in the hole dominated devices, such as: interfacial state at organic/metal, charge traps by the defects in the real devices and the surface dipole related interfacial electronic structure changes.[6,7] However, because the injection current is proportional to $\exp(-q\varphi_B/kT)$, where q is an electron charge, φ_B the injection barrier, k the Boltzmann constant, and T the temperature. When the injection barrier is reduced by 0.15 eV, the injection current at room temperature ($kT \approx 0.026$ eV) would be increased by 2 orders of magnitude.

3.3. Device Stability. The lifetime of Devices A, B, and C, operated at 20 mA/cm^2, are shown in Figure 7. For better comparison, the measured lifetimes at different initial luminance are converted into the same luminance by an empirical equation[34]

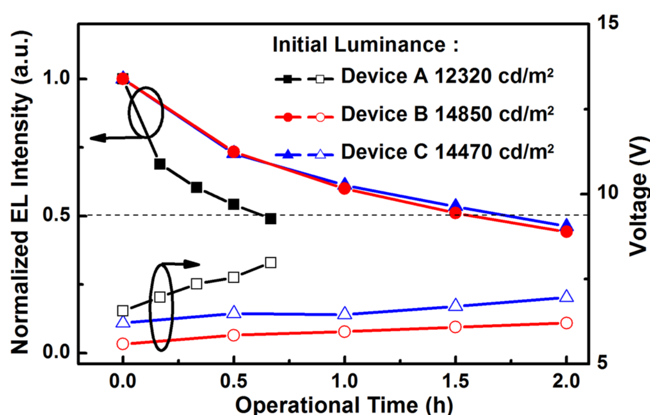

Figure 7. Normalized EL intensity and voltage rise as a function of operational time at 20 mA/cm^2.

$$T_{50}(L) = T_{50}(L_0)\left(\frac{L_0}{L}\right)^{1.5} \quad (1)$$

where $T_{50}(L)$ is the lifetime converted at an initial luminance of L and $T_{50}(L_0)$ is the real lifetime at the initial luminance of L_0. According to the empirical equation, the comparable lifetime at the initial luminance of 1000 cd/m^2 is 27, 89, and 94 h for Devices A, B, and C, respectively. The lifetime of Device B with 1 nm $InCl_3$ is three times longer than that of Device A with only UV-ozone treatment, and is comparable to that of Device C with CF_x plasma treatment. Meanwhile, Device B has the smallest voltage rise of about 0.63 V, whereas that for Devices A and C corresponds to 1.41 and 0.75 V, respectively. The evaluation of dark spots growth in the three devices is also carried out. There were no noticeable changes in the density and size of dark spots in the three devices before and after the lifetime tests. It suggests that the degradation of all devices must be caused by mechanisms other than reaction with atmosphere, such as: (1) effect of the device fabricating circumstance;[5] (2) chemical interaction such as oxidation between ITO and adjacent organic materials;[22] (3) indium diffusion from ITO to the excitons combination area under operation;[35] (4) crystallization of organic materials.[24] Combined with present devices, all of the three devices are fabricated at the same time with identical conditions. It is therefore suggested that chemical interaction, indium diffusion and crystallization were the main degradation factors in Device A. With a treatment of UV-ozone, the concentration of oxygen near the ITO surface will be increased, resulting in the oxidation of adjacent organic material.[8,9,22,36] Lee et al. also reported that the efficiency and stability of OLEDs were affected strongly by the indium diffusion from ITO to the excitons combination zone under operation.[35] Because of large energy offset at the interface of ITO/CBP,[24] defect states induced by the crystallization of organic film may act as carrier traps and recombination centers, leading to the device degradation. For Device C, the prolonged lifetime is mainly attributed to a dipole generation at the ITO/CF_x interface because of reduced energy level offset at anode/organic interface.[19] For Device B, we ascribed its good stability to the lower driving voltage owing to lowered barrier height and enhanced hole injections due to In−Cl bond formed at the ITO/$InCl_3$ interface. The lower voltage drop at the ITO/CBP interface avoids a large amount of joule heat, which would suppress the crystallization of CBP material, and thus improve the device stability. It is well-known that the In−Cl bond is stronger than the In−O bond. Therefore, Cl can immobilize the In atom more effectively and suppress the diffusion of In atoms into the organic layer under operation. And thus Device B exhibits the good stability. The result agrees with the previous work using ITO anode treated by Cl_2 plasma.[24,37]

There are several factors to affect the lifetime of OLEDs, especially PHOLEDs. Our study demonstrates that $InCl_3$ modification provides a more stable ITO/organics interface than UV-ozone plasma treatment, leading to a more reliable operation of OLEDs. Modifying the ITO surface with $InCl_3$ is one of many ways to improve the anode interface and to enhance the device lifetime. If the other interfaces could also be carefully designed with suitable materials and layer structures, the lifetime of the devices would be further increased.

dx.doi.org/10.1021/am3011324 | ACS Appl. Mater. Interfaces 2012, 4, 5211−5216

4. CONCLUSIONS

A simple method of modifying the anode surface of ITO by thermally evaporating an ultrathin $InCl_3$ film has been developed. The work function of ITO can be significantly improved by 0.48 eV through direct formation of $In^{3+}-Cl^-$ bond at the ITO surface compared with the case of UV-ozone treatment. A fitting of the temperature-dependent $J-V$ curves by Schottky thermal emission model shows that the hole barrier in the device with $InCl_3$ modification is reduced by 0.15 eV compared with the device without $InCl_3$. And at least 2 orders of magnitude of improvement in current density are observed in the device with $InCl_3$ at the same voltage and the identical temperature. For EL performance, 36% improvement of power efficiency and more than three times extension of lifetime have been realized in a simplified trilayer green phosphorescent OLED with ITO anode modified by 1 nm $InCl_3$. The improved EL performance is mainly attributed to the lowered hole injection barrier at the anode/organic interface owing to the generation of dipoles at the ITO/$InCl_3$ interface resulting from rich and negatively charged chlorine. Our results suggest that the ITO/$InCl_3$ anode is an excellent choice to enhance the hole injection in OLEDs.

■ ASSOCIATED CONTENT

Ⓢ Supporting Information

The current density−voltage−luminance curves, the current efficiency−current density curves, the power efficiency-current density curves, the normalized EL intensity−-wavelength curves of PHOLEDs with different $InCl_3$ layer thicknesses of 0, 0.5, 1, 1.5, and 2 nm. The log−log scale plot of current density−voltage curves of OLED Devices A, B, and C. The SEM morphologies of the ITO surface without $InCl_3$ and with 1 nm $InCl_3$. This material is available free of charge via the Internet at http://pubs.acs.org/.

■ AUTHOR INFORMATION

Corresponding Author

*E-mail: lsliao@suda.edu.cn (L.-S.L.); zkwang@suda.edu.cn (Z.-K.W.).

Notes

The authors declare no competing financial interest.

■ ACKNOWLEDGMENTS

We acknowledge financial support from the Natural Science Foundation of China (61036009, 61177016, and 21161160446), the National High-Tech Research Development Program (2011AA03A110), the Natural Science Foundation of Jiangsu Province (No.BK2010003). This is also a project funded by the Priority Academic Program Development of Jiangsu Higher Education Institutions (PAPD).

■ REFERENCES

(1) Tang, C. W.; VanSlyke, S. A. *Appl. Phys. Lett.* **1987**, *51*, 913−915.
(2) Xiao, L.; Chen, Z.; Qu, B.; Luo, J.; Kong, S.; Gong, Q.; Kido, J. *Adv. Mater.* **2011**, *23*, 926−952.
(3) Liao, L. S.; Slusarek, W. K.; Hatwar, T. K.; Ricks, M. L.; Comfort, D. L. *Adv. Mater.* **2008**, *20*, 324−329.
(4) Zhou, D. Y.; Cai, S. D.; Gu, W.; Liao, L. S.; Lee, S. T. *Appl. Phys. Lett.* **2010**, *97*, 223302.
(5) Wang, Z. K.; Lou, Y.; Naka, S.; Okada, H. *ACS Appl. Mater. Interfaces* **2011**, *3*, 2496−2503.
(6) Wang, Z. K.; Lou, Y.; Naka, S.; Okada, H. *Appl. Phys. Lett.* **2011**, *98*, 063302.
(7) Wang, Z. B.; Helander, M. G.; Qiu, J.; Puzzo, D. P.; Greiner, M. T.; Liu, Z. W.; Lu, Z. H. *Appl. Phys. Lett.* **2011**, *98*, 073310.
(8) Ding, X. M.; Hung, L. M.; Cheng, L. F.; Deng, Z. B.; Hou, X. Y.; Lee, C. S.; Lee, S. T. *Appl. Phys. Lett.* **2000**, *76*, 2704−2706.
(9) Sugiyama, K.; Ishii, H.; Ouchi, Y.; Seki, K. *J. Appl. Phys.* **2000**, *87*, 295−298.
(10) Ishida, T.; Kobayashi, H.; Nakato, Y. *J. Appl. Phys.* **1993**, *73*, 4344−4350.
(11) Zhu, L.; Tang, H.; Harima, Y.; Yamashita, K.; Aso, Y.; Otsubo, T. *J. Mater. Chem.* **2002**, *12*, 2250−2254.
(12) Van Slyke, S. A.; Chen, C. H.; Tang, C. W. *Appl. Phys. Lett.* **1996**, *69*, 2160−2162.
(13) Kondakova, M. E.; Young, R. H.; Prosperi, D. A.; Miller, R. L.; Comfort, D. L. *SID'10 Dig.* **2010**, 1808−1811.
(14) Chan, I. M.; Hsu, T. Y.; Hong, F. C. *Appl. Phys. Lett.* **2002**, *81*, 1899−1901.
(15) Zhu, X. L.; Sun, J. X.; Peng, H. J.; Meng, Z. G.; Wong, M.; Kwok, H. S. *Appl. Phys. Lett.* **2005**, *87*, 153508.
(16) Wang, F.; Qiao, X.; Xiong, T.; Ma, D. G. *Org. Electron.* **2008**, *9*, 985−993.
(17) Son, M. J.; Kim, S.; Kwon, S.; Kim, J. W. *Org. Electron.* **2009**, *10*, 637−642.
(18) Groenendaal, L.; Jonas, F.; Freitag, D; Pielartzik, H.; Reynolds, J. R. *Adv. Mater.* **2000**, *23*, 481−494.
(19) Hung, L. S.; Zheng, L. R.; Mason, M. G. *Appl. Phys. Lett.* **2001**, *78*, 673−675.
(20) Tang, J. X.; Li, Y. Q.; Zheng, L. R.; Hung, L. S. *J. Appl. Phys.* **2004**, *95*, 4397−4403.
(21) Zhou, X.; Pfeiffer, M.; Blochwitz, J.; Werner, A.; Nollau, A.; Fritz, T.; Leo, K. *Appl. Phys. Lett.* **2001**, *78*, 410−412.
(22) Scott, J. C.; Kaufman, J. H.; Brock, P. J.; DiPietro, R.; Salem, J.; Goitia, J. A. *J. Appl. Phys.* **1996**, *79*, 2745−2751.
(23) Helander, M. G.; Wang, Z. B.; Qiu, J.; Greiner, M. T.; Puzzo, D. P.; Liu, Z. W.; Lu, Z. H. *Science* **2011**, *332*, 944−947.
(24) Cao, X. A.; Zhang, Y. Q. *Appl. Phys. Lett.* **2012**, *100*, 183304.
(25) Nefedov, V. I.; Zhumadilov, E. K.; Kopytova, T. Yu. *J. Struct. Chem* **1977**, *18*, 549−533.
(26) Briggs, D. *Handbook of X-Ray and Ultraviolet Photoelectron Spectroscopy*; Heyden and Son Ltd.: London, 1977; Chapter 7.
(27) Beerbom, M. M.; Lägel, B.; Cascio, A. J.; Doran, B. V.; Schlaf, R. *J. Electron Spectrosc. Relat. Phenom.* **2006**, *152*, 12−17.
(28) Schlaf, R.; Murata, H.; Kafafi, Z. H. *J. Electron Spectrosc. Relat. Phenom.* **2001**, *120*, 149−154.
(29) Gmeiner, J.; Karg, S.; Meier, M.; Riess, W.; Strohriegl, P.; Schwoerer, M. *Acta Polym.* **1993**, *44*, 201−205.
(30) Lou, Y.; Wang, Z.; Naka, S.; Okada, H. *Appl. Phys. Lett.* **2011**, *99*, 033305.
(31) Scott, J. C. *J. Vac. Sci. Technol., A* **2003**, *21*, 521−531.
(32) Shen, Y.; Klein, M. W.; Jacobs, D. B.; Scott, J. C.; Malliaras, G. G. *Phys. Rev. Lett.* **2001**, *86*, 3867.
(33) Sze, S. M. *Physics of Semiconductor Device*, 2nd ed.; Wiley: New York, 1981; Chapter 5.
(34) Liao, L. S.; Ren, X.; Begley, W. J.; Tyan, Y. S.; Pellow, C. A. *SID'08 Dig.* **2008**, 818−821.
(35) Lee, S. T.; Gao, Z. Q.; Hung, L. S. *Appl. Phys. Lett.* **1999**, *75*, 1404−1406.
(36) Mason, M. G.; Hung, L. S.; Tang, C. W.; Lee, S. T.; Wong, K. W.; Wang, M. *J. Appl. Phys.* **1999**, *86*, 1688−1692.
(37) Zhang, Y. Q.; Acharya, R.; Cao, X. A. *J. Appl. Phys.* **2012**, *112*, 013103.